

# Lattice contrast in the core-loss EFTEM signal of graphene

Michael J. Mohn\*, Johannes Biskupek, Zhongbo Lee, Harald Rose, Ute Kaiser\*

*Materialwissenschaftliche Elektronenmikroskopie, Universität Ulm, Albert-Einstein-Allee 11, 89081 Ulm, Germany*

## ARTICLE INFO

### Keywords:

Energy-filtered transmission electron microscopy  
High-resolution transmission electron microscopy  
Atomic-resolution imaging  
Preservation of elastic contrast  
Mutual coherence function  
Two-dimensional materials

## ABSTRACT

The realization of chromatic aberration correction enables energy-filtered transmission electron microscopy (EFTEM) at atomic resolution even for large energy windows. Previous works have demonstrated lattice contrast from ionization-edge signals such as the  $L_{2,3}$  edges of silicon or titanium. However, the direct interpretation as chemical information was found to be hampered by contributions from elastic contrast with dynamic scattering, especially for thick samples. Here we demonstrate that even for thin samples with light atoms, the interpretation of the ionization-edge signal is complicated by inversions from bright-atom to dark-atom contrast. Our EFTEM experiments for graphene show lattice contrast in the carbon K-edge signal, and we find bright-atom and dark-atom contrast for different defoci.

## 1. Introduction

Correction of the spherical aberration ( $C_s$ ) in high-resolution transmission electron microscopy (HRTEM) allows atomic-resolution imaging at typical electron energies of 80 to 300 keV. Additional correction of the chromatic aberration  $C_c$  leads to a drastic improvement in the capabilities to elucidate structural and chemical properties of the samples. Firstly, the resolution of the  $C_c/C_s$ -corrected microscope is further improved by reducing the dampening effect of the chromatic defocus spread  $\sigma(C_1)$  [1], and  $C_c/C_s$  correction enables atomic resolution at even lower electron energies  $E_0$ , e.g., 20–80 keV [2]. Secondly, energy-filtered TEM (EFTEM) experiments can be conducted with large energy windows  $\Delta E$ , yielding a point resolution and information limit that suffice for obtaining lattice contrast from ionization edges [3].

Using a  $C_c/C_s$ -corrected microscope, Urban et al. [4] and Forbes et al. [5] have obtained lattice contrast from the Si- $L_{2,3}$  ionization edge of Si and from the Ti- $L_{2,3}$  and the O-K ionization edges of Sr-TiO<sub>3</sub>, respectively. Both experimental works notice the preservation of elastic contrast and the necessity to incorporate this effect in the interpretation of the data. In fact, inelastic scattering is always accompanied by simultaneous elastic scattering [6], and coherent interference between elastically scattered waves forms elastic contrast, also known as phase contrast. Contributions from elastic scattering to the inelastic signal in EFTEM images are also known from theoretical investigations [7–9] and dedicated spectroscopy experiments [10]. Many image simulations suggest, however, that the direct interpretation as pure chemical maps can still work for samples thinner than about one third of the extinction length (threshold for dynamic scattering), usually a few nanometers

and less [5,8,9,11].

In this paper, we investigate experimentally if ionization-edge EFTEM images of a two-dimensional object can be directly interpreted as atomic-resolution elemental maps, using the low-voltage  $C_c/C_s$ -corrected SALVE (Sub-Angstrom Low-Voltage Electron Microscopy, [12]) instrument. We have chosen graphene as a one atom thin object and evaluate its EFTEM signals. For comparison of different energy-filtered signals, we present energy-filtered images from the zero loss, the plasmon loss, and the carbon K (C-K) edge of graphene. Among these images, the zero loss (ZL) image is our reference for elastic contrast. It corresponds to the phase-contrast image known from HRTEM and shows either bright-atom or dark-atom contrast, depending on the defocus. The plasmon-loss images are also expected to show only preserved elastic contrast, as the plasmon-loss scattering itself is highly delocalized [13,14] with its characteristic scattering angles being 100 times smaller than for elastic scattering. Eventually, in the case of the C-K-edge images, the inelastic scattering is much more localized, and that we can expect actual lattice contrast from the inelastic scattering itself. This inelastic contrast is expected to be bright-atom contrast—with the carbon atoms being self-luminous, bright point sources that can only be imaged sharply at optimum focus. This bright-atom contrast is crucial for the interpretation of the ionization-edge image as an elemental map, where high intensity indicates the presence of a certain element. Any contributions with dark-atom contrast will obscure the elemental map and hamper the direct interpretation of the ionization-edge images.

\* Corresponding authors.

E-mail addresses: [michael.mohn@uni-ulm.de](mailto:michael.mohn@uni-ulm.de) (M.J. Mohn), [ute.kaiser@uni-ulm.de](mailto:ute.kaiser@uni-ulm.de) (U. Kaiser).

<https://doi.org/10.1016/j.ultramic.2020.113119>

Received 7 February 2020; Received in revised form 14 August 2020; Accepted 13 September 2020

Available online 19 September 2020

0304-3991/ © 2020 Elsevier B.V. All rights reserved.

## 2. Methods

### 2.1. Experiments

The high-resolution EFTEM experiments were carried out at an acceleration voltage of 80 kV using the  $C_c/C_s$ -corrected SALVE instrument. This microscope is based on a Thermo Fisher Titan Themis<sup>3</sup> column and is equipped with a dedicated aberration corrector from CEOS company [2,12]. Chromatic aberrations were corrected to values that allow for imaging with sub-Ångström resolution even for energy windows as large as 20 eV. The parameters were  $C_c = -5 \mu\text{m}$  (to compensate partly for the third-order  $C_{3c}$  fixed at 16 mm), chromatic first-order astigmatism  $A_{1c} < 1 \mu\text{m}$ , and chromatic dispersion  $W_c < 1 \mu\text{m}$ . The geometric aberrations up to  $A_5$  and  $S_5$  were tuned to allow for a phase plate of 50 mrad ( $\pi/4$  criterion), including a  $C_s/C_5$  optimization with a small negative value of  $C_s$  at  $-5 \mu\text{m}$  compensating  $C_5$  of 3 mm and allowing maximum phase-contrast transfer.

TEM samples of clean, free-standing graphene were prepared by transferring commercially available graphene on copper foils (CVD grown by Graphenea company, Spain) to Quantifoil holey carbon grids (Quantifoil company, Germany). Atomically clean graphene areas of approx.  $20 \times 20 \text{ nm}^2$  were first identified from zero-loss-filtered images. EFTEM images and electron energy-loss spectroscopy (EELS) signals were recorded on the camera (Ultrascan 1000 XP) of the GIF Quantum ERS low-voltage imaging energy filter attached to the SALVE microscope. The energy filter was tuned to provide non-isochromaticity below 1 eV and a chromatic distortion of 0.3%, both measured over the whole camera area.

For the acquisition of core-loss EFTEM images, a 20 eV EFTEM energy window was centered around 300 eV high-tension offset, such that a large part of the carbon K-edge signal contributes to the EFTEM image [cf. EELS signal in Fig. 1(a)]. As the ratio between the C-K-edge signal and the elastic signal in the zero-loss peak is only about  $1:10^4$ , an

extraordinarily high electron dose of about  $10^9 \text{ e}^-/\text{nm}^2$  was needed to achieve sufficient signal-to-noise ratio (SNR) in the core-loss EFTEM images. This was achieved with a largely condensed illumination with a diameter slightly larger than the camera's field of view, and exposure times of 4 s. The total beam current was 20 nA, limited by the electron source (monochromated X-FEG). The condenser-lens focus (illuminated area) and the beam deflectors were controlled by the energy-filter software to compensate for beam shifts and intensity changes caused by the high-tension offsets for EFTEM with 300 eV energy loss. Unfortunately, this automated setting does not compensate for introduced beam tilts, which may cause coma and astigmatism in the EFTEM images. To minimize this deleterious effect, the rotation center of the objective lens was re-adjusted at 300 eV high-tension offset.

On binned  $1024 \times 1024$  pixel frames on the  $2048 \times 2048$  pixel CCD, the electron dose of  $10^9 \text{ e}^-/\text{nm}^2$  resulted in an average of about 100 counts per pixel (conversion rate of 15 counts per 80 kV primary electron). This low usable dose of less than  $10^5 \text{ e}^-/\text{nm}^2$  makes the graphene lattice hard to see in the raw data, as shown in Fig. 1(b). This raw image also shows the inhomogeneity of the condensed illumination, resulting in a strong intensity gradient in the image. The high intensity at the left edge of the image stems from carbon contamination on the graphene. In the Fourier transform of the raw image [Fig. 1(c)], however, graphene's first-order Bragg reflections are clearly visible.

As the electron dose in the EFTEM image is about 1000 times larger than typically used for high-resolution TEM images of graphene, severe damage in the form of nanometer-sized holes was observed after 1–2 minutes of sample illumination. As a consequence, we could record only a few single-exposure core-loss images, and an averaging over multiple unit cells of graphene was necessary in post-processing to evaluate the contrast of the high-resolution EFTEM images. A detailed description of the image processing procedure is given in the Appendix.

A background subtraction with two or more pre-edge windows was not performed, as the signal in 20 eV windows directly in front of the C-K-edge onset (284 eV [15]) was below the noise level. Along with the C-K post-edge EFTEM images, we have recorded zero-loss-filtered and plasmon-loss images (6–26 eV) at each sample position.

### 2.2. Image simulations

For comparison to our EFTEM experiments, we have performed image simulations using the mutual coherence function (MCF), including both elastic and inelastic scattering. Inelastic scattering transfers energy from the scattered electron to the object, entangling the scattering electron with the states of the object. In this case, it is not possible to describe the scattered wave by a single wave function, as it is the case for the elastically scattered wave. Instead, we must describe the outgoing wave as a collection of partial waves, each corresponding to a specific excited state. Only partial waves pertaining to the same excited state are coherent. For a given energy loss, the partial coherence between the inelastically scattered electrons can be described by a density matrix [16] or by the MCF [12,17]. Since each plane wave is represented by a two-dimensional vector, the corresponding density matrix or the MCF entangling two plane waves are four-dimensional quantities. Multiple scattering involving inelastic scattering is either modelled by the Bloch-wave formalism [7] or by the multislice algorithm [18]. In the multislice algorithm, the propagation of the four-dimensional MCF through the sample as well as through the components of the microscope inevitably requires time-consuming 4D Fourier transforms to be performed for each energy loss and for each slice. Hence, the 4D Fourier transforms are converted to combinations of more computationally efficient 2D Fourier transforms, for which there are several methods [7,10,19–21]. In this work, we simplify the computation by representing the 4D matrices using their primary 2D eigenvectors retrieved from matrix diagonalization [22]. The number of the used 2D Fourier transforms depends on the required computational accuracy.

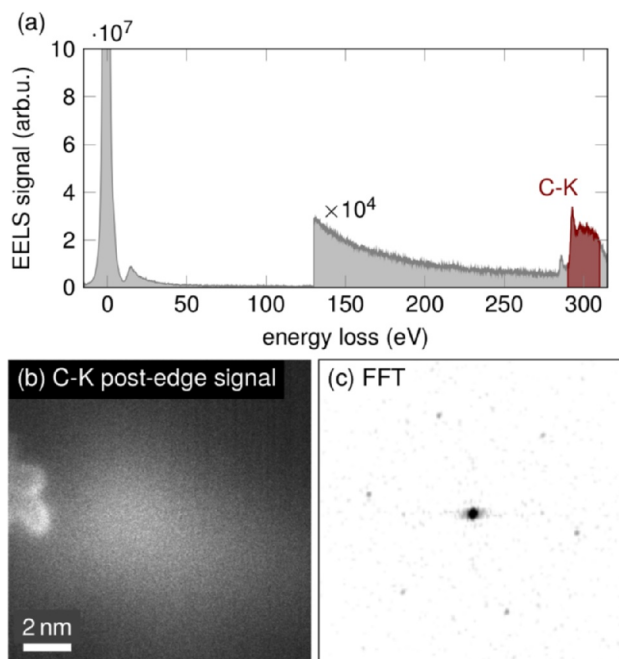


**Fig. 1.** (color online) (a) EELS signal of single-layer graphene: zero-loss peak (ZLP) and carbon K-shell (C-K) ionization edge. The selected energy window for the EFTEM experiments is highlighted in red. Note that the high-loss signal  $> 130 \text{ eV}$  was enhanced by a factor of  $10^4$ . (b) Raw 80 kV EFTEM signal from the C-K edge of graphene, recorded with a 20 eV energy window centered at 300 eV energy loss. Due to the low signal-to-noise ratio, the graphene lattice is not directly visible. (c) Fast Fourier transform of the raw EFTEM signal from (b), showing first-order reflections of graphene (cropped, contrast enhanced).

We carry out the EFTEM image simulations in two steps: First, the interaction between the electrons and the sample is modeled by the mutual coherence multislice algorithm [18]. In the case of graphene, mutual coherence multislice reduces to a single slice, and we assume that both elastic and inelastic scattering take place simultaneously. For low energy losses in the range of 6–26 eV, we replace one 4D Fourier transform by one 2D Fourier transform. For high energy losses in the range of 290–310 eV, however, we have to take multiple eigenvectors into account and replace one 4D Fourier transform by a number of two-dimensional Fourier transforms. As a result, in the low and high energy-loss regions, the outgoing waves are represented by 10 partial wave and by 30 partial waves, respectively. The propagation of the 2D partial waves through the microscope column is similar to the case of elastic scattering. For a given energy window, images for the respective energy losses are first simulated individually, and are subsequently summed up after multiplication with a weighting factor obtained from the normalized EELS spectra. The zero-loss images are simulated following the procedure in Ref. [23], and the applied MATLAB code to carry out the EFTEM simulations is available upon request by contacting the authors.

In order to account for the partial spatial coherence of the rather converged electron beam during the core-loss EELS experiments, a large illumination convergence semiangle of 2 mrad was used in the simulations.

### 3. Results

Our processed EFTEM images show either bright-atom or dark-atom contrast, within a small focus range. Fig. 2 shows two sets of zero-loss (ZL) and C-K-edge EFTEM images of graphene. The underlying raw images were recorded at optimized conditions for the C-K-edge images; that is, focusing and stigmation of the objective lens were performed with the help of the live Fourier transform of the raw post-edge images. Only the first-order graphene reflections could be used as reference for stigmation, as no Thon fringes were present. Fig. 2(a) shows a ZL-filtered image of pristine graphene with bright-atom contrast. This ZL-filtered image was averaged over the same number of graphene unit

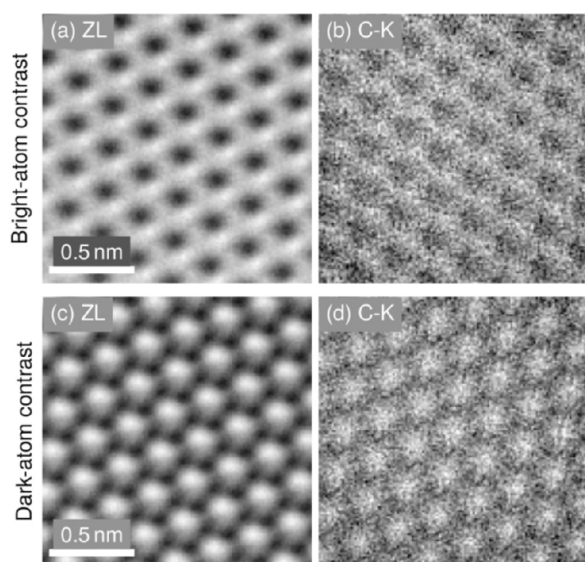


**Fig. 2.** Bright-atom and dark-atom contrast in 80 kV high-resolution EFTEM images of graphene: (a,b) Processed zero-loss (ZL) and C-K post-edge EFTEM images with bright-atom contrast. (c,d) Another experiment at different defocus, resulting in dark-atom contrast in the ZL and C-K edge images; All images were taken under optimized conditions for the C-K-edge signal, with 20 eV windows centered at 0 eV (ZL) and 300 eV (C-K). For the shown images, raw signals were averaged over more than 100 unit cells to improve the signal-to-noise ratio.

cells as the corresponding post-edge-filtered image in Fig. 2(b). Fig. 2(a,b) both show bright-atom contrast, but with a much stronger signal in the ZL-filtered (elastic) image. At different defocus, both images change contrast similarly from bright-atom to dark-atom contrast, as presented in Fig. 2(c,d). We were able to reproduce these results at different sample positions. Depending on the defocus, the ZL-filtered and C-K-edge images both show either bright-atom or dark-atom contrast. Remarkably enough, the contrast never flipped between the ZL-filtered and C-K-edge image in any of our experiments.

For a systematic investigation of the defocus dependency of the C-K post-edge signal, we have recorded EFTEM focus series. As a starting point, we have used a defocus that yields maximum lattice contrast in the raw signal and varied the focus in the range of -20 to +20 nm in steps of 2 nm. For the discrimination between bright-atom and dark-atom contrast, the signals were again averaged over a large number of unit cells. In a narrow defocus range, we have found the contrast changing repeatedly between bright- and dark-atom contrast. This is demonstrated in Fig. 3(a), where exemplary images at relative defocus offsets of up to  $\pm 8$  nm around the optimum focus for bright-atom contrast ( $C_{1,opt}$ ) show a change from dark atoms to bright atoms and vice versa. At much higher defocus offsets, the lattice contrast was lost, which became apparent by missing graphene reflections in the Fourier transform of the raw images, and by vanishing contrast in the averaged images.

We are now comparing our experimental focus series to image calculations [Fig. 3(b)], which show very similar contrast changes in the same focus range around a calculated optimum defocus  $C_{1,opt} = +3$  nm for bright-atom contrast. Please note that we do not aim for a perfect contrast matching but rather for a qualitative agreement between the experiments and simulations. During the focus series acquisition, it was impossible to monitor all experimental parameters such as, e.g., introduced astigmatism or coma at 300 eV energy loss, or the influence of drift on the exact focus steps. Given, in addition, the low SNR in the raw (unprocessed) experimental images, a one-to-one comparison between individual images is not sensible.

As a reference for preserved elastic contrast in energy-loss signals, we have also performed EFTEM experiments in the low-loss region of the EELS spectrum. Due to the high delocalization of the inelastic scattering in the plasmon-loss region ( $\sim 16$  eV), only elastic scattering is expected to yield lattice resolution. Fig. 4(a) shows a focus series recorded with the plasmon-loss electrons in graphene (6–26 eV). Again, the focus series covers a defocus range of  $\pm 8$  nm around the optimum focus for bright-atom contrast in (phase-contrast) high-resolution TEM. Under these conditions, we find that the experimental plasmon-loss series show a very similar behavior as the C-K-edge focus series from Fig. 3. Within defocus changes of 6–8 nm, the contrast again changes from dark-atom contrast to bright-atom contrast and vice versa. Qualitatively, we can again confirm this by image simulations [Fig. 4(b)], especially for negative defocus offsets. Deviations between the experimental images and the image simulations for certain defoci may be partly caused by the change in high tension from 300 eV offset down to 16 eV, and the associated change in the imaging conditions.

For a closer investigation of the similarities between the C-K-edge and plasmon-loss signals, we have also performed EFTEM image simulations for isolated carbon atoms. With simulated focus series, we again analyze the defocus behavior of the EFTEM signals. Fig. 5 shows the simulated focus series for the plasmon-loss and C-K-edge signals of single C atoms. In Fig. 5(a), the plasmon-loss signals (6–26 eV) are shown using the same brightness and contrast settings for all defoci between -8 nm and +8 nm. Horizontal line scans across the center of each image are shown as blue curves. Likewise, the corresponding carbon K-edge signals (290–310 eV) are shown in Fig. 5(b).

Looking at the plasmon-loss signals, we find that the simulations for single C atoms readily shows a clear change between bright-atom contrast and dark-atom contrast. As is the case of an elastic zero-loss image, the C atom can appear either brighter or darker than the

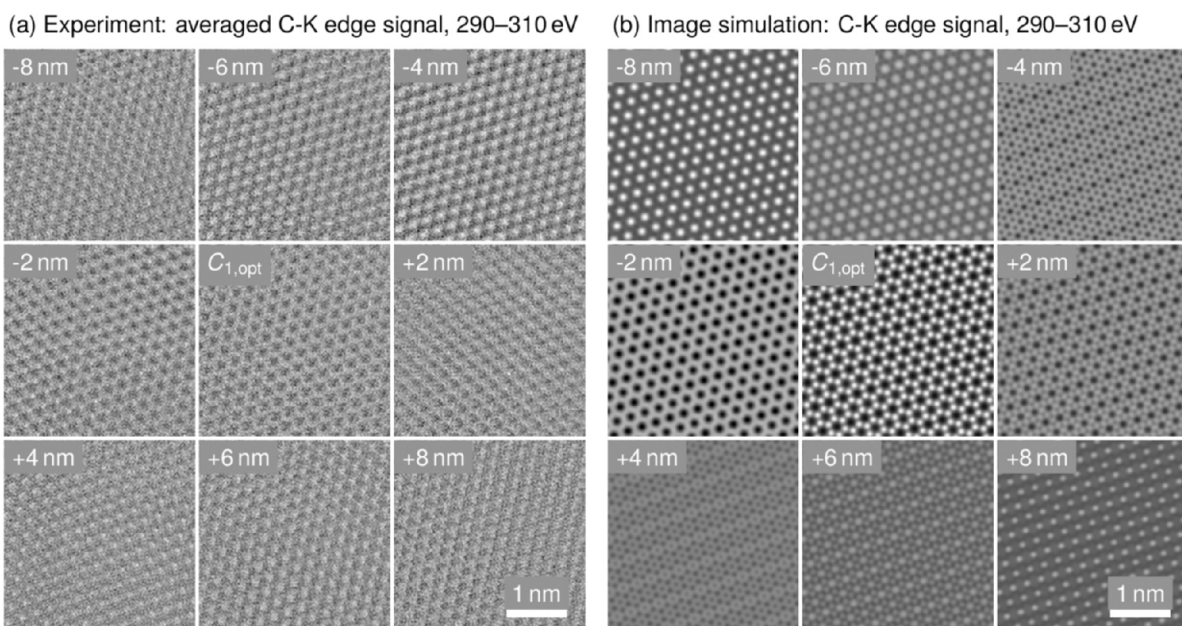


**Fig. 3.** Focus series with 80 kV high-resolution EFTEM signal from the C-K edge of graphene (20 eV window centered at 300 eV): Images taken with defocus offsets between  $-8$  and  $+8$  nm show an inversion of contrast from dark-atom contrast to bright-atom contrast and vice versa. The images are post-processed by averaging over more than 100 unit cells to improve the signal-to-noise ratio.

nonzero background signal. As opposed to this, the C-K-edge signals of the isolated atoms always appear bright on a dark background with zero intensity. For deviations from the optimum defocus  $C_{1,opt}$ , the width of the C-K-edge signal is broadened to an extent that no true atomic resolution can be obtained for graphene. In fact, the signals have a full width at half maximum (FWHM) way beyond the atomic spacing of  $1.4$  Å, such that the intensity would be spread over multiple atomic sites. In the case of positive defocus offsets, we even find ring-shaped intensity profiles that can cause the signal in-between the atoms to actually become stronger than that at the atomic sites themselves. These broad intensity distributions around the atoms can also favor dark-atom contrast in our EFTEM experiments and image simulations

for graphene. This is illustrated in the bottom row of Fig. 5(b), where the simulated C-K-edge images of single carbon atoms are incoherently summed up, which can also result in graphene images with dark-atom contrast.

#### 4. Conclusions

We have presented lattice contrast in 80 kV EFTEM images from the C-K ionization edge of graphene and compare them to zero-loss filtered and plasmon-loss images, as well as image simulations. Our results obtained for graphene, a one atom thin layer of carbon ( $Z = 6$ ), show that atomic resolution EFTEM data cannot be directly interpreted in

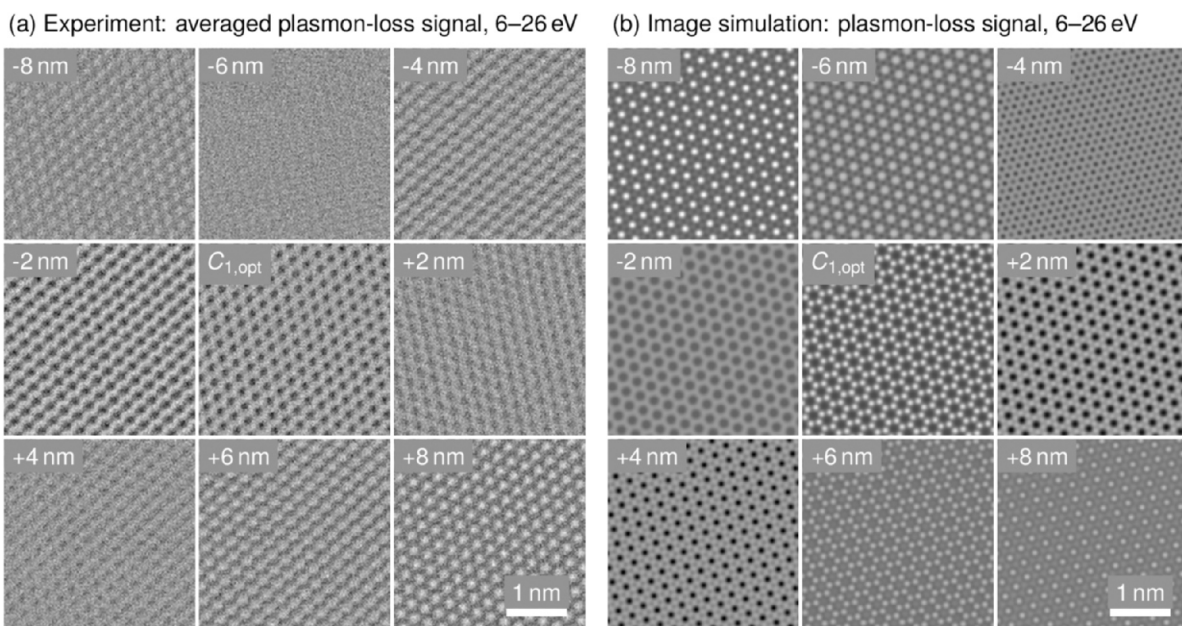


**Fig. 4.** Focus series with 80 kV high-resolution EFTEM signal from the plasmon loss of graphene (20 eV window centered at 16 eV): Images taken with defocus offsets between  $-8$  and  $+8$  nm show an inversion of contrast from dark-atom contrast to bright-atom contrast and vice versa. The images are post-processed by averaging over more than 100 unit cells to improve the signal-to-noise ratio.

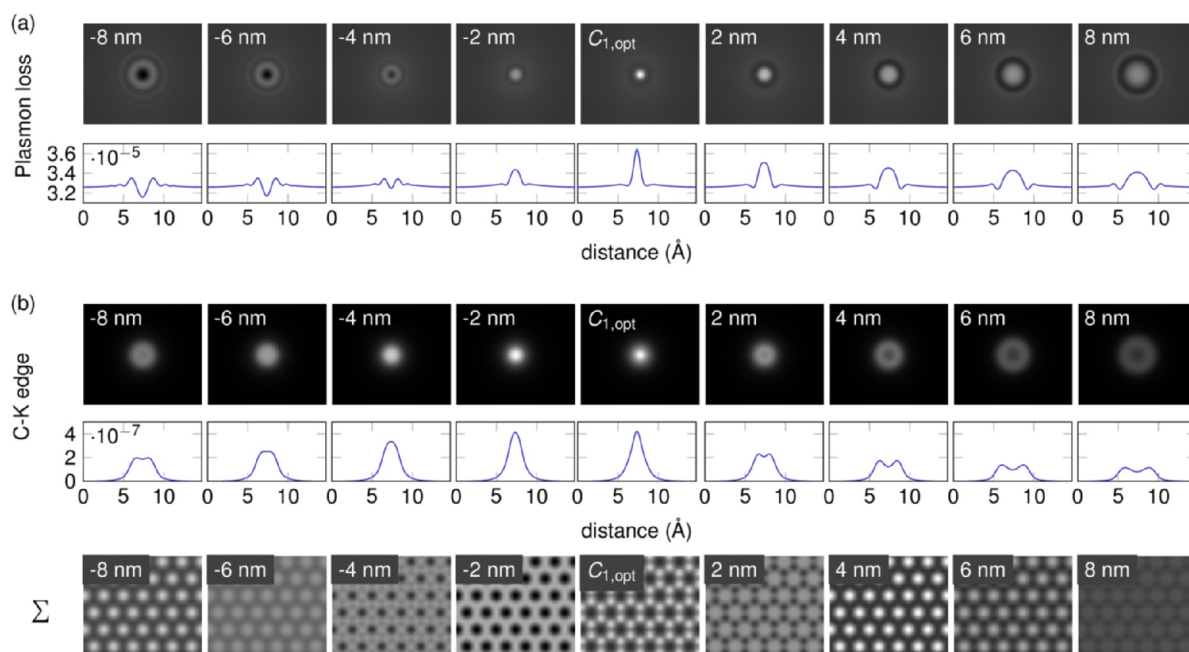


**Fig. 5.** (color online) EFTEM image simulations for single carbon atoms: Plasmon loss (a) and C-K edge (b). The blue curves show horizontal line scans across the center of the images. The additional images in (b) show the sum of the single-atom signals, forming graphene images with bright-atom contrast or dark-atom contrast.

terms of chemical contrast. Depending on the defocus, we have obtained images with either bright-atom contrast or dark-atom contrast. This finding puts into question the widespread assumption that chemical information can be still be directly obtained for very thin samples, where multiple scattering is unlikely. In practice, lattice-resolution EFTEM will not always result in elemental maps with bright atoms.

In focus series of the C-K-edge EFTEM signal, we have observed very similar contrast inversions as in the (preserved) elastic contrast in the plasmon-loss signal. We find that this behavior can have different reasons. On the one hand, even the ionization-edge signal can—in principle—show preserved elastic contrast. In particular, we can qualitatively reproduce our focus series with image calculations using the mutual coherence function (MCF), which always include elastic scattering. On the other hand, the defocused C-K-edge signal of a single, isolated carbon atom can already have a rather broad intensity distribution beyond the atomic spacing in graphene. In EFTEM images of graphene, this can still yield lattice resolution, but may cause contrast inversions from bright-atom contrast to dark-atom contrast.

Our findings demonstrate the complications in atomic-resolution elemental mapping by EFTEM, even in  $C_c/C_s$ -corrected TEM. For elemental mapping on the atomic scale, other techniques may have clear advantages over EFTEM, such as the new method of energy-filtered

imaging scanning TEM [24,25] where image contrast was even shown to be stable with changing sample thickness [25]. Also, in STEM-EELS, at least the contributions from elastic contrast are less prominent, as demonstrated by experiments with graphene [26].

#### Declaration of Competing Interest

The authors declare that they have no known competing financial interests or personal relationships that could have appeared to influence the work reported in this paper.

#### Acknowledgments

We want to thank Dr. Heiko Müller and Dr. Martin Linck from CEOS company for valuable discussions on the EFTEM experiments. The authors acknowledge funding from the German Research Foundation (DFG) and the Ministry of Science, Research and the Arts of the federal state of Baden-Württemberg, Germany in the frame of the SALVE project (DFG project number 270370833). Further, we acknowledge funding from the DFG in the frame of the OMNI project (Orbital Mapping Near Interfaces, DFG project number 423465915).

#### Appendix. Image processing

In post-processing, all lattice-resolution EFTEM images of graphene were averaged over a large number of unit cells to enhance the signal-to-noise ratios (SNRs) of the raw signals.

In a first step, outliers (e.g., hot and dead pixels) were identified via their absolute and relative deviation from the median intensities of the surrounding pixels. For deviations above certain thresholds, pixel intensities were replaced by the median of the surroundings. The strong intensity gradients caused by the relatively inhomogeneous illumination were compensated by subtracting Gaussian blurred versions of the images, which has an effect similar to highpass filtering. From the binned frames with  $1024 \times 1024$  pixels, small sub-regions with the highest signal-to-noise ratio were cropped and used for the evaluation.

For the actual summation over multiple unit cells, the direct-space graphene lattice was determined from the maxima in the autocorrelation of a zero-loss filtered image at same magnification. This lattice was then used as a kernel for a convolution with the preprocessed core-loss images, leading to an averaging over a large number of unit cells (see Fig. 6). The final results were cropped to the size of the kernel to avoid artifacts from the image borders.

As an alternative to the above-described averaging technique, the bright-atom and dark-atom contrasts could in principle also be revealed by Fourier filtering of the raw images. To this end, small circular masks can be placed around each spot in the fast Fourier transforms (FFTs), including the central spot with the low-frequency information. Keeping only the signal from the masked areas, this leads to very similar results with respect to

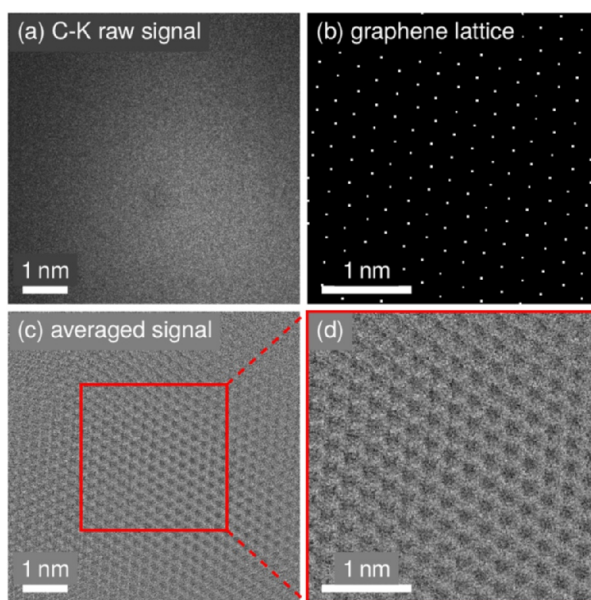


**Fig. 6.** (color online) Averaging of the graphene C-K-edge EFTEM signal over multiple unit cells. (a) Raw C-K-edge EFTEM signal; (b) Graphene lattice as obtained from a zero-loss image; (c) Averaged signal by convolution of (a,b); (d) Magnified region from (c).

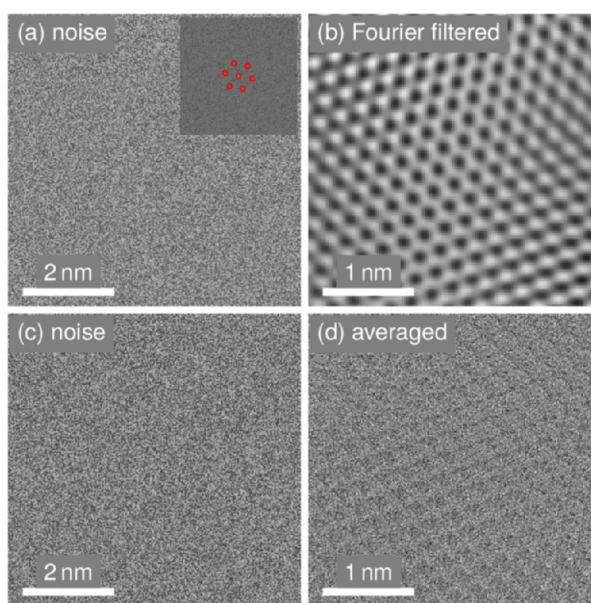


**Fig. 7.** (color online) Comparison of periodic artifacts from Fourier filtering (a,b) and from averaging over multiple unit cells (c,d), using random noise as input data. (a) Random noise and hexagonal filter mask in the Fourier transform [inset]. (b) Fourier-filtered image with a deceptively clear bright-atom contrast at the center. (c,d) Random noise before and after averaging over multiple unit cells. The averaged signal in (d) shows only weak periodic artifacts.

the discrimination between bright- and dark-atom-contrast images. In contrast to the averaging technique, however, this can yield deceptively clear bright-atom or dark-atom contrast images even for vanishingly low signal. This is exemplified in Fig. 7, where both the averaging and the Fourier-filtering method are applied to computer-generated random noise. In contrast to the very clear hexagonal lattice introduced by the Fourier filtering [Fig. 7(b)], the averaging technique yields only weak periodic artifacts [Fig. 7(d)].

## References

- [1] M. Haider, P. Hartel, H. Müller, S. Uhlemann, J. Zach, *Microscopy and Microanalysis* 16 (2010) 393–408.
- [2] M. Linck, P. Hartel, S. Uhlemann, F. Kahl, H. Müller, J. Zach, M. Haider, M. Niestadt, M. Bischoff, J. Biskupek, Z. Lee, T. Lehnert, F. Börrnert, H. Rose, U. Kaiser, *Physical Review Letters* 117 (2016) 076101.
- [3] B. Kabius, P. Hartel, M. Haider, H. Müller, S. Uhlemann, U. Loebau, J. Zach, H. Rose, *Journal of Electron Microscopy* 58 (2009) 147–155.
- [4] K.W. Urban, J. Mayer, J.R. Jinschek, M.J. Neish, N.R. Lugg, L.J. Allen, *Physical Review Letters* 110 (2013) 185507.
- [5] B.D. Forbes, L. Houben, J. Mayer, R.E. Dunin-Borkowski, L.J. Allen, *Ultramicroscopy* 147 (2014) 98–105.
- [6] H. Rose, *Ultramicroscopy* 15 (1984) 173–191.
- [7] A. Howie, *Proceedings of the Royal Society of London, Series A. Mathematical and Physical Sciences* 271 (1963) 268–287.
- [8] P. Stallknecht, H. Kohl, *Ultramicroscopy* 66 (1996) 261–275.
- [9] T. Navidi-Kasmai, H. Kohl, *Ultramicroscopy* 81 (2000) 223–233.
- [10] K. Kimoto, Y. Matsui, *Ultramicroscopy* 96 (2003) 335–342.
- [11] J. Verbeeck, P. Schattschneider, A. Rosenauer, *Ultramicroscopy* 109 (2009) 350–360.

- [12] "SALVE III project, [www.salve-project.de](http://www.salve-project.de)", visited on June 10, 2020.
- [13] D.A. Muller, J. Silcox, *Ultramicroscopy* 59 (1995) 195–213.
- [14] R.F. Egerton, *Ultramicroscopy* 180 (2017) 115–124.
- [15] C. C. Ahn, O. L. Krivanek, R. P. Burger, M. M. Disko, and P. R. Swann, EELS atlas (HREM Facility, Center for Solid State Science, Arizona State University; Gatan, Inc., Tempe, Arizona; Warrendale, PA, 1983).
- [16] P. Schattschneider, M. Nelhiebel, B. Jouffrey, *Phys. Rev. B* 59 (1999) 10959.
- [17] H. Rose, *Optik* 45 (1976) 139–158.
- [18] H. Müller, H. Rose, P. Schorsch, *Journal of Microscopy* 190 (1998) 73–88.
- [19] C. Dwyer, *Ultramicroscopy* 151 (2015) 68–77.
- [20] N. Lugg, B. Freitag, S.D. Findlay, L.J. Allen, *Ultramicroscopy* 110 (2010) 981–990.
- [21] S. Löffler, V. Motsch, P. Schattschneider, *Ultramicroscopy* 131 (2013) 39–45.
- [22] Z. Lee, R. Hambach, U. Kaiser, H. Rose, *Ultramicroscopy* 175 (2017) 58–66.
- [23] Z. Lee, J.C. Meyer, H. Rose, U. Kaiser, *Ultramicroscopy* 112 (2012) 39–46.
- [24] H.G. Brown, A.J. D'Alfonso, B.D. Forbes, L.J. Allen, *Ultramicroscopy* 160 (2016) 90–97.
- [25] F.F. Krause, A. Rosenauer, J. Barthel, J. Mayer, K. Urban, R.E. Dunin-Borkowski, H.G. Brown, B.D. Forbes, L.J. Allen, *Ultramicroscopy* 181 (2017) 173–177.
- [26] M.D. Kapetanakis, W. Zhou, M.P. Oxley, J. Lee, M.P. Prange, S.J. Pennycook, J.C. Idrobo, S.T. Pantelides, *Phys. Rev. B* 92 (2015) 125147.